The Detailed Structure of the Tropical Upper Troposphere and Lower Stratosphere as Revealed by Balloonsonde Observations Of Water Vapor, Ozone, Temperature and Winds During The NASA TCSP And TC4 Campaigns

Henry B. Selkirk[1], Holger Vömel[2], Jessica María Valverde Canossa[3], Leonhard Pfister[4], Jorge Andrés Diaz[5], Walter Fernández[5], Jorge Amador[6,5],Werner Stolz[7], Grace Peng[8]

[1]Goddard Earth Sciences and Technology Center, University of Maryland-Baltimore County, NASA Goddard Space Flight Center, Greenbelt, MA USA

[2]Deutscher Wetterdienst, Meteorologisches Observatorium, Lindenburg, Germany

[3]School of Environmental Sciences, National University, Heredia, Costa Rica

[4]Earth Sciences Division, NASA Ames Research Center, Moffett Field, CA USA

[5]School of Physics, University of Costa Rica, San José, Costa Rica

[6]Center for Geophysical Research, University of Costa Rica, San José, Costa Rica

[7]National Meteorological Institute, San José, Costa Rica

[8]The Aerospace Corporation, Los Angeles, CA USA

Submitted to the Special Section on the NASA TC4 Misison
of the Journal of Geophysical Research – Atmospheres
September 17, 2009

Contact information:
Dr. Henry Selkirk
Goddard Earth Sciences and Technology Center
University of Maryland Baltimore County
Code 613.3, NASA Goddard Space Flight Center
Greenbelt, MD 20771
e-mail: Henry.B.Selkirk@nasa.gov
tel: (301) 614-6846 fax: (301) 614-5903

Abstract

Balloonsonde measurements of water vapor and ozone using the Cryogenic Frostpoint Hygrometer (CFH) and electrochemical concentration cell (ECC) ozonesondes were made at Alajuela [10.0°N, 84.2°W] during two NASA airborne campaigns: the Tropical Convective Systems and Processes (TCSP) mission in July 2005 and the Tropical Composition Clouds Climate Coupling (TC4) mission, July-August 2007. In addition high resolution radiosondes were launched four times daily at the same site from mid-June through mid-August in both years. The upper troposphere was frequently saturated, sometimes in layers with stratospheric levels of ozone and at other times with low ozone indicative of uplifted tropospheric layers, and dehydration near the cold point tropopause (CPT) was observed in many profiles. Both ozone and water vapor displayed large increases of variability above 350 K due to upward propagation of mixed Rossby-gravity waves. As a result of these waves, CPT water vapor saturation mixing ratios from the radiosonde record varied from less than 2 to greater than 8 ppmv, and CFH water vapor measurements at the CPT show a similar range about a mean of 5.8 ppmv for the two campaigns. Despite the large temporal variability in cold point water vapor mixing and saturation mixing ratios, it is found that dehydration of nascent stratospheric air occurred no higher than a kilometer above the mean level of the CPT at 16.6 km and ~375 K. This dehydration is predominantly the result of cooling in forced ascent by the equatorial waves in concert with overall upwelling in the upper troposphere.

1. Introduction

The means by which water vapor is transported into the tropical lower stratosphere has been a very lively subject of debate since *Danielsen* [1982] and *Newell and Gould-Stewart* [1981 presented different views of the relative roles of deep convection and of larger-scale lifting and radiative heating in tropical stratosphere-troposphere exchange (STE). These papers were motivated in part by the observations of the annual cycle of tropical tropopause temperature and its relationship to the spatial and seasonal distribution of deep convection in the tropics [*Reed and Vleck,* 1969; *Reid and Gage,* 1981; *Yulaeva et al.,* 1994; *Reid and Gage*, 1996]. However, it was *Mote et al.* [1996] who first conclusively showed that the annual cycle of the temperature at the tropical tropopause imprints a coherent signal on the water vapor content in the tropical stratosphere. This observation and subsequent refinements using much longer satellite records impose powerful constraints on estimates not only of the tropical upwelling rate and the mixing into the tropics from the middle latitudes [*Mote et al.,* 1998; *Schoeberl et al.,* 2008], but also on estimates of the effective mixing ratio of water as it passes irreversibly through the tropical tropopause and enters the tropical stratospheric 'pipe' [*Plumb and Ko,* 1992].

Despite these advances in our understanding of the large-scale circulation in the tropical stratosphere, the remoteness and coldness of the tropical tropopause environment make difficult direct observation of the physical processes that lead to dehydration and STE. Nevertheless, as shown by *Wang et al.* [1996], thin cirrus is present at or near the tropopause over large regions of the tropics year round, and work by *Gettelman et al.* [2002] and *Liu and Zipser* [2005] demonstrated that deep convective ascent to and through the tropical tropopause is a relatively rare event. These observations provide support for a range of stratosphere-troposphere exchange processes occurring on scales greater than the convective. For example, *Sherwood and Dessler* [2001] advocated a mix of convective overshooting and subsequent lofting at larger scales. Recently, *Corti et al.* [2006] have investigated upwelling in large convective anvil systems, and the dehydration of layers hydrated upstream by deep convection and lifted by large-scale ascent or tropical waves has been studied by *Jensen et al.* [1996], *Hartmann et al.* [2001], *Holton and Gettelman* [2001], and *Pfister et al.* [2001].

Vömel et al. [2002] analyzed balloonsonde measurements of water vapor and ozone at diverse locations in the tropics, including the western Pacific warm pool, the eastern equatorial Pacific, and South America. They found supersaturation in the upper troposphere under a wide range of conditions and concluded that tropopause dehydration was occurring not only due to rapid ascent in deep convective systems, but also through slow ascent and lifting by the passage of Kelvin waves [*Fujiwara et al.,* 2001].

In this paper we report on two extended campaigns of balloon-borne measurements of water vapor and ozone launched from the radiosonde site of the National Meteorological Institute of Costa Rica (IMN) at Alajuela [10.0°N, 84.2°W]. These accompanied the NASA Tropical Convective System and Processes (TCSP) airborne mission in July 2005 [*Halverson et al.,* 2007] and the NASA Tropical Composition, Cloud and Climate Coupling (TC4) experiment in July and August 2007 [*Toon et al.,* this issue]. During these two campaigns a total of 38 soundings were made with a payload that included the University of Colorado cryogenic frostpoint hygrometer (CFH) [*Vömel et al.,* 2007a] and an ECC ozonesonde [*Komhyr et al.,* 1995]. The CFH is recognized as a reference instrument for water vapor measurements in the cold environment near the tropical tropopause and in the lower stratosphere and displays excellent agreement with the Aura MLS satellite water vapor measurement [*Vömel, et al.,* 2007b].

The TCSP and TC4 campaign CFH/ECC datasets provide an unprecedented opportunity to examine the short timescale variability of the structure of water vapor and ozone in the tropical upper troposphere and lower stratosphere (UT/LS) during periods of widespread regional convection. We place our analysis in the context of the evolution of the dynamical structure of the UT/LS using four-times-daily radiosondes launched from the IMN site in campaigns concurrent with the water vapor and ozone balloonsondes. These radiosonde data allow us to examine the dominant role of convectively-driven equatorial waves in the variation of the local tropical tropopause temperature and the control of the effective water vapor mixing ratio of air entering the stratosphere in the region.

Highwood and Hoskins [1998] introduced the term Tropical Tropopause Layer (TTL) to highlight the depth of the transition from the troposphere to the stratosphere in the tropics and the range of physical processes that determine its vertical structure. Inasmuch as the TTL is inherently a statistical entity defined in terms of temporal and spatial averages, in this study we do not try to refine the definition of the TTL *per se*; our data are limited to one location and to one particular time of the year. For this reason we will we refrain from interpretation of particular features in our analysis in terms of the "TTL", and will use the more general term UT/LS to refer to the layer encompassing the tropical cold point tropopause (CPT). Nevertheless, the temperature, water vapor and ozone profile data examined here speak strongly to the nature of the variability within the TTL, independent of its definition.

In Section 2 of this paper we describe the balloonsonde and radiosonde data presented in the paper. Section 3 examines the mean structure and variability of temperature, ozone and water vapor from the CFH/ECC sondes in the two campaigns, while Section 4 focuses on the detailed structure of six representative balloon soundings in the TCSP campaign. In Section 5 we examine wave-induced variability in the UT/LS and its relationship to tropopause temperature using the radiosonde temperature and wind data. Section 6 summarizes the results and presents conclusions.

2. Data

The Ticosonde/Aura-TCSP (TCSP) balloonsonde project ran from June through August 2005, and the Ticosonde/TC4 project June through August 2007. Each consisted of two concurrent balloonsonde campaigns with launches from Juan Santamaria International Airport, Alajuela, Costa Rica [10.0°N, 84.22°W]: (a) a series of CFH/ECC balloonsondes to measure profiles of water vapor and ozone, typically near local noon but also with night flights, and (b) a program of 4-times daily radiosonde launches. The latter began in mid-June and spanned periods of at least two months while the intensive water vapor and ozone profiling took place over periods of two-and-one-half weeks and a month respectively with 23 CFH/ECC ascents during TCSP and 15 during TC4.

a. Water vapor-ozone balloonsondes

Profiles of water vapor and ozone to the middle stratosphere were measured with a balloon payload combining the CFH with the ECC ozonesonde; a Garmin GPS provided winds. The CFH is a lightweight (400-g) microprocessor-controlled instrument and operates on the chilled-mirror principle using a cryogenic liquid as cooling agent. It includes several improvements over the similar NOAA/CMDL instrument [*Vömel et al.,* 2002] allowing it to measure water vapor continuously from the surface to about 28 km altitude. The accuracy in the troposphere is better than 5%, and the stratospheric accuracy is better than 10%. The CFH is capable of measuring water vapor inside clouds, but may occasionally suffer from an artifact in which the optical detector collects water or ice. This condition leads to a malfunction of the instrument controller that is easily identified, and thus can be screened out of the processed data.

The ECC ozonesonde measures ozone by reaction with I_2 in a weak aqueous solution, the electrical current generated being directly proportional to the amount of ozone pumped through the cell. The accuracy of the ozone mixing ratio is typically ~5% and slightly lower at low ozone mixing ratios.

During flight the CFH, ECC and GPS data streams were transmitted to the ground-receiving equipment through an interface with a Vaisala RS80 radiosonde; the latter's PTU data stream was also captured. A Vaisala RS92-SGP was also added to the payload for the purposes of inter-comparison of the RS92 twin-humicap relative humidity (RH) measurement with that from the CFH. As reported previously by *Vömel et al.* [2007c] this revealed a dry bias of the RS92-SGP relative humidity due to solar radiation approaching 50% at 15 km.

The full CFH/ECC payloads weighed approximately a kilogram and were flown from a 1200-g latex balloon filled with helium. Each balloon was equipped with a parachute so that data could be taken on descent as well as allow for the potential recovery of the instruments. Payload preparation and sonde launches were conducted by a team of students from the National University (UNA) of Costa Rica under the leadership of two of us (Vömel and Valverde). The UNA team was assisted by IMN technical staff.

The CFH/ECC launches in the 2005 TCSP campaign were made on 18 consecutive days near local noon beginning July 8. On each of the last five days of the campaign, ascents were also made near local midnight. All but three ascents reached altitudes of 27 km or more, the highest altitude being 32.2 km. Twenty of the 23 flights had good water vapor ascent data above 10 km, and on 14 of these we obtained good data through the profile temperature minimum or higher. An initial launch for TC4 was made at local noon on July 2, 2007, but the intensive phase of the 2007 TC4 campaign began on July 16 with local noon launches every 3 days through July 31 with an additional 8 flights through August 13, four of them taking place at local midnight. We have also included the noon launch on August 30 in our analysis. Table 1 lists the dates, times and maximum altitudes of ascent data achieved in each of the flights.

b. Radiosondes

The Ticosonde Aura-TCSP radiosonde launch campaign ran from 00 UT June 16 through 00 UT August 24. 269 of the flights reached the 150 hPa level or higher for an average burst altitude of 25.6 km. The great majority of the ascents were made with the Vaisala RS92-SGP radiosonde, although in the final days of the campaign these were substituted with Vaisala RS90-AG sondes on 19 occasions and the Vaisala RS80-15G sonde on 5 occasions. The Ticosonde/TC4 campaign in 2007 also began at 00 UT on June 16 but ran through 15 August 2007, with twice-daily (00 and 12 UT) launches in June, and four-times daily (00, 06, 12 and 18 UT) beginning July 1. Vaisala RS92-SGP sondes were launched throughout. 207 of the 214 flights reached 150 hPa or higher and of these the average burst altitude was 30.9 km.

The ground receiving equipment at the Alajuela station was a Vaisala MW11 upgraded prior to the 2005 campaign for reception of the RS92 digital signal. Sonde preparation, the balloon launches and telemetry were carried out by IMN staff with assistance of students from the University of Costa Rica (UCR). Approximately half the time we used 600-g latex balloons filled with helium. For the remaining launches we used 500-g balloons filled with hydrogen. See the Appendix for a discussion of the Ticosonde collaborative program.

3. Average profiles and variability from the water vapor and ozone soundings

We calculated the mean profiles and variance for temperature, ozone volume mixing ratio, observed and saturated water vapor volume mixing ratio, and relative humidity over ice (RHi) from the CFH/ECC sonde ascent data. To calculate mean statistics, we interpolated each ascent to a 50-m altitude grid and then derived means, standard deviations, as well as the maximum and minimum at each grid level in each campaign sample.

a. Temperature structure

The results for temperature and ozone mixing ratio are shown in Figures 1a (TCSP) and 1b (TC4). Table 2 tabulates statistics for variables at the CPT for both campaigns. In terms of the average values, maxima and minima for the variables shown in Table 2, the CPTs in the two campaigns differed only slightly, although the variability is somewhat lower in TC4. Thus in round numbers, the CPT on average lay at 100 hPa, 375 K potential temperature and an altitude of 16.6 km. These values are well within a standard deviation of the global average values for July in the tropical tropopause climatology of *Seidel et al.* [2001].

The mean CPT water vapor mixing ratio for the two campaigns was close to 5.8 ppmv and the ozone mixing ratio was ~150 ppbv. We note that the latter is some 50 ppbv higher than the mean ozone at 100 hPa in the analysis by *Fueglistaler et al.* [2009] of the SHADOZ data [*Thompson et al.,* 2003]. 100 hPa lies close to 375 K in their Figure 2a, so we infer that the CPT in our data is embedded in a layer that *on average* contains a significant admixture of stratospheric air. How much this statistical characteristic represents irreversible mixing of stratospheric and tropospheric air is not clear, however, the individual profiles that we will discuss in Section 4 may offer some clues.

The mean TCSP temperature profile stabilizes at 15.1 km, 130 hPa and 357 K; here N^2 increases from 1.58 to 3.7 x 10^{-4} s^{-2}; similar behavior is observed in TC4. However, the most striking feature of the temperatures in both campaigns is the sharp increase of temperature variability above the 355 K level, shown in both in Figure 1 in terms of temperature range (light gray profiles at right) and as variance in Figure 2a. This is especially pronounced in TC4 due to the strong inversions observed in the first week of August. Thus while in the middle and upper troposphere below 15 km the full range of temperatures in the TCSP sample is nowhere greater than 4.2°C, it increases to over 12°C by 16.5 km, close to the mean cold point. Above this level and up to the limit of our data above 31 km, the variability remains significantly higher than its values in the free troposphere. This will be discussed in more detail in Section 4.

b. Ozone

The mean profiles of ozone differ in the troposphere where there is 25-35% more ozone during TC4 than in TCSP and the variance is greater as is shown in Fig. 2b. However both mean profiles show inflections at 350 K, and while the TC4 variance does not display the abrupt increase at 350 K seen in TCSP, the 350 K level during TC4 lies within a steep variance gradient beginning at ~345 K. Thus in both instances increases in ozone variance accompany the inflections in the mean profile. Folkins *et al.* [2002] and others have linked the latter to a transition from detrainment of low ozone air by the deepest convective clouds to a regime where the ozone balance is between vertical advection and chemical production. The large temperature variance however is a strong indication that while this may be a layer of limited convective mixing, it is nonetheless extremely dynamic.

c. Water vapor

Figure 3 displays the CFH water vapor volume mixing ratio data for each flight series and their mean profiles along with profiles of saturation water vapor mixing ratio and relative humidity over ice. The saturation mixing ratio is derived from the Vaisala RS80 pressure and temperature data using the Goff-Gratch formula for the saturation vapor pressure over ice [*Goff and Gratch,* 1946]. For display purposes we have smoothed these profiles with an 11-pt boxcar filter. We also plot the envelope of ±1 standard deviation of the water vapor, similarly smoothed. Finally, we plot the mean cold point in pressure and water vapor space. At right in each panel we have plotted the smoothed mean profile of relative humidity over ice within its envelope of ± 1 standard deviation.

Above 5 km (a level at or very close to the 0°C point in each campaign) the vertical structure of the water vapor structure was characterized by an unsaturated layer between

5 and 10 km with a mean RH_i of 50-75% and frequent instances of very dry air (RH_i < 10%), a nearly saturated upper tropospheric layer with saturation frequently exceeding 140% or more between 12 and 16 km, and above 16 km a layer encompassing the CPT. In the latter, the mean RHi and the incidence of supersaturation decline rapidly.

Kley *et al.* [1982] first showed that the minimum water vapor volume mixing ratio in this region and season is not located at the tropopause but well into the stratosphere. Table 3 presents statistics of the water vapor minima for the two campaigns. It lay somewhat lower than TC4 during TCSP at 19.5 km, 62.1 hPa, and 451.6 K potential temperature with value of 3.2 ppmv. The respective values for TC4 were 20.3 km, 54.3 hPa, 476.7 and 3.0 ppmv. Standard deviations of at the profile minima (0.47 and 0.56 ppmv respectively) were similar.

As can be seen in Figure 2c, in both campaigns the vertical structure of the variability of water vapor is generally opposite to that observed in temperature and in ozone, with a rapid drop in the upper troposphere above ~335 K (~8 km) and a leveling off between 350 and 360 K. The large range of values of water vapor tend to obscure fine aspects of this vertical structure, so we have also plotted the standard deviations normalized by the mean profile. We call this the fractional deviation, and both the TCSP and TC4 profiles of this quantity maximize in the upper troposphere, roughly defining the layers of the maximum frequency of supersaturation observations. Above 355-360 K the fractional deviation profiles have secondary peaks in each campaign, a broad one in TCSP peaking just below the mean cold point and a narrower one in TC4 at and just above the mean cold point; the latter is co-located with a local maximum in temperature variability. Thus the strong increase of variability of temperature and ozone above 350 K is paralleled by concomitant structure in the variability in the water vapor, and the vertical motions that are modulating temperature and ozone are very likely controlling water vapor in this region. Below 350 K quite the opposite is true and water vapor variability is de-coupled from lifting and sinking motions due to wave motions and more related to convective cloud activity limited to the troposphere below 350 K layer.

The profile of maximum saturations in Figure 3 (right) suggests an upper limit for cold-trapping of air that is entering the stratosphere locally. In both campaigns this level is close to the mean cold point (16.8 km in TCSP, 17.1 km in TC4). In TC4 this maximum cold trap altitude is just 450 meters below the highest cold point in the sample while in TCSP it is more than a kilometer lower. Figure 4 offers a more detailed look at the variability in the neighborhood of this level and the stratospheric content of this air. It displays the complete RHi data for the two campaigns plotted against height. To distinguish air of stratospheric origin from tropospheric air we color-coded each point according to its mixing ratio. The center in each color bar is the maximum in each campaign observed below the 345 K potential temperature level; for TCSP this was 65 ppbv and in TC4 91 pbbv. The left-hand extremum in each color bar is the tropospheric (*i.e.* sub-345 K) average value.

Figure 4 shows that frequent supersaturation above 300 hPa and up to the 350 K level was observed in both campaigns. The ozone mixing ratios suggest that these saturated layers are tropospheric. The layer above 350 K is on the other hand heterogeneous with stratospheric (deep green) parcels found at all levels and strongly tropospheric (deep red) parcels up to 15 km. Significantly, however, air with tropospheric ozone levels is not observed within 200-300 m of the mean cold point level.

Above the cold point, the envelope of RHi values in Figure 4 shows how quickly the atmosphere dries out even within the altitude range of the observed cold points. In TCSP, except for the cluster of points between 81 and 73 hPa all observed on flight SJ009, 50% RHi is not observed above 85 hPa, 17.5 hPa and 400 K and 75% not above 17 km. In TC4 75% RHi is only observed above 17.2 km, and on one flight.

The results in Figure 4 demonstrate that if "writing" to the atmospheric water vapor tape recorder requires that air parcels both dehydrate and be stratospheric in ozone content, then the so-called 'tape head' occurs in a layer below the highest level of observed saturation. In TCSP this level was 16.8 km and 384 K and in TC4, 17.1 km and 388 K. Using the above criterion and our ozone and relative humidity data, tape writing could have been occurring as low as 353.7 K and 15.0 km in TCSP and 349 K and 13.6 km in TC4. In terms of the mean relative humidity profiles in each campaign, and the SHADOZ threshold of 100 ppbv for stratospheric air mentioned earlier, a lower boundary could defined at 15.6 km and 361.4 K in TCSP and 15.4 km and 360.9 K in TC4. Using this latter definition, we would locate a 'regional' tape head in a layer above 360 K and below 390 K, not significantly different from the range suggested by *Schoeberl et al.* [2006] and *Read et al.* [2004] using MLS data for the whole tropics. Given the frequency of supersaturation at the mean CPT and its rapid fall above, however, it is more likely that in this region, an excellent estimate effective mixing ratio of air entering the stratosphere is afforded by the mean water vapor at the CPT; at ~5.8 ppmv it is a good 2 ppmv lower than the values close to 8 ppmv at the lower boundary of the tape head 'layer.'

4. Characteristics of individual water vapor and ozone profiles

Figure 5 shows six profiles from the TCSP campaign that represent a range of behavior in water vapor mixing ratio, ozone mixing ratio, saturation mixing ratio and RHi. As in Figure 3, we have color-coded the water vapor points according to RHi, and the campaign mean profiles of both water vapor mixing ratio and ozone mixing ratio are plotted to highlight regions of positive and negative anomalies. In our discussion, we will refer to dehydration or hydration of the tropopause when a saturated layer at or above the mean CPT has a minimum value less or greater than the campaign mean.

The profiles for July 11 (a) and July 19 (d) stand out as examples of strong dehydration at or very close to the CPT, reaching 2.34 ppmv at 16.6 km on July 11 and 2.68 ppmv at 16.2 km on July 19. Both of these cold and dry tropopauses are anomalously low in ozone for those levels, yet under the working definition of tropospheric air we adopted for Figure 4, the ozone mixing ratios in the layers are marginally stratospheric. The anomalously low ozone extends down to 15.3 km in the first case and to nearly12 km in the second; both are supersaturated. The atmosphere immediately above the tropopause in each case shows not only a strong inversion in saturation mixing ratio (and equivalently temperature) but also an extremely steep gradient in ozone mixing ratio, as much as 500 ppbv/km on July 19. This gradient is conistent with upward motion and adiabatic cooling below and descent of stratospheric air above.

The sounding from July 13 (Figure 5b) in (b) shows supersaturation both in the upper troposphere between 12 km and 15 km and in the layer near the CPT. The upper layer contains stratospheric levels of ozone that are greater than the campaign mean, and the upper boundary of the layer lies above 380 K. It is possible that this combination of the supersaturation, stratospheric ozone and high potential temperature was produced by penetrating convection, but wave motions could have produced this as well. Soundings c and e (July 16 and 23 respectively) are subsaturated except for shallow layers near the tropopause. In the July 16 case, subsaturation in the upper troposphere from 13-15 km is accompanied by relatively elevated ozone levels. While the subsaturation is too small to indicate descent from the stratosphere, it does indicate subsidence. Sounding f (July 25) like b, c, and e, shows no significant tropopause dehydration, and an upper troposphere with relatively high ozone. Futhermore, stratospheric levels of ozone appear as low as 14.5 km; below this subsaturated layer the air is strongly supersaturated down to nearly 12 km with ozone discontinuities both at the top and bottom of the latter layer.

5. Temperature variability and coherent fluctuations in the upper troposphere and the lower stratosphere

We have shown in Section 3 that in both campaigns the variability of temperature and ozone increases substantially above the 350 K potential temperature level, dramatically so in the case of TCSP. Here we show that the dominant modes of temperature variability above this level during both TCSP and TC4 lie in a spectrum of equatorial waves that are most likely excited by the deep convection in the region. *Pfister et al.* [this issue] found that during the summer of 2007 when TC4 took place, these waves included modes on time scales of a week or more as well as higher frequency inertio-gravity waves. Here we focus on the wave variability observed during TCSP, during which the longer period modes were more dominant than in TC4.

Upward propagation of equatorial waves is sensitive to wind shear. Figure 6 shows the profiles of the radiosonde mean zonal and meridional wind derived from the four-times daily radiosonde launches at Alajuela for the 61days between 00 UT June 16 through 18 UT August 15, 2005; the mean profiles are bracketed by envelopes of ±1 standard deviation. The profiles were obtained by interpolating the 2-sec data from each sounding to a 10-m grid and then calculating mean profiles on this grid.

The wind profiles in Figure 6 can be compared with the very similar features of the TC4 wind profiles in *Pfister et al.* [*op. cit.*], *viz.*, east-southeasterly winds above the boundary layer that become easterly and then east-northeasterly, above 9 km in this case. The winds in 2005 also show increased variability in both components in the upper troposphere and mean northeasterly flow in the uppermost troposphere. The primary difference between 2005 and 2007 is that this upper tropospheric flow is stronger and extends through the mean cold point level. In the stratosphere there is a similarly strong easterly shear that culminates in an easterly wind maximum of 42 ms^{-1} at 30 km.

Figure 7 displays time-height cross-sections of temporal anomalies of the radiosonde temperature (T), zonal wind (u) and meridional wind (v) for the same period as in Figure 6. Before plotting we took each grid-level time series and subtracted the 61-day mean and removed any linear trend. In addition the data in the figures was smoothed in the vertical using a 101-pt boxcar smoother. For reference purposes we also plot the campaign mean heights of CPT and the 350 and 355 K potential temperature levels, and in addition along the bottom edge of each plot arrows at the times of the 23 ascents of the CFH/ozonesonde payload between July 8 and 25.

Figure 7a is the time-height cross-section of the T anomalies. While there is very little coherent variation below 350 K, above this level and up to at least 21 km, there is an unmistakable pattern of downward propagating anomalies at periods of 4-16 days and vertical wavelengths of 4-5 km. In the Figure we drawn dashed and dotted phase lines to highlight the descending cold and warm anomalies. The largest temperature anomalies occur between 355 K and the level of the mean CPT, though anomaly amplitudes of 4 K occur on several occasions near the 24-km level.

Figures 7b and c show time-height cross-sections of u and v anomalies respectively. Both show very different behavior in the troposphere below 355 K where anomalies are vertically aligned; in the lower troposphere easterly wave pulses of the meridional wind are particularly regular. In the UT/LS the meridional wind appears to be in phase with the temperature anomalies, *i.e.,* cold anomalies are accompanied by northerly wind anomalies while the zonal wind anomalies appear to be in quadrature.

As these waves impact the temperature at the tropopause, they have an effect on the saturation mixing ratio of water vapor. Figure 8 shows the time series of the saturation mixing ratio at the CPT during the 2005 campaign. (*Pfister et al.* [*op. cit.*] present the corresponding time series for the summer of 2007.) The time series exhibits both high-frequency variability and peak-to-peak variations of up to 4 ppmv at time scales of ~5 days mixed with periods twice that; these become prominent after an extended low period in the first 10 days of the record (mid-to late June). We have also plotted in Figure 8 the shorter record of water vapor mixing ratios from the gridded CFH sounding data (July 8-25). As we have already shown in the previous section, the cold point during TCSP was more often than not supersaturated. Thus it is not surprising to note that the water vapor measurements in almost all cases exceed the saturation mixing ratio. Nevertheless the sense of the synoptic scale variations in the saturation mixing ratio time series is preserved in the CFH data; in particular there are saturation mixing ratio minima near days 192 and 201 that correspond to the strongly dehydrated profiles on July 11 and 19.

The results of spectral analyses of T, u and v are shown in Figure 9. They support the inferences from Figures 6 and 8. First, centered at 16 km, *i.e.,* somewhat below the mean level of the CPT, the temperature shows a peak at periods centered at 4 days and a broader peak centered between 8 and 16 days. The 4-day feature extends upward through the CPT to just above 18 km as does power at periods longer than 16 days. Above 25 km there is considerable power at a wide range of time scales longer than the inertial period (2.88 days at 10° latitude), but relatively little power between 20 and 25 km except for weak feature in the 20-22 km region at ~5 days. Neither the zonal or the meridional wind show as much spectral power at the tropopause and above relative to their variability in the troposphere, despite the clear features appearing in the time-height cross-sections in Figure 7. However, the zonal wind power is dominated in the upper troposphere by roughly the same periods as the temperature shows at the tropopause and the lower stratosphere; and the meridional wind shows a particularly strong feature at 4 days shifted only slightly downward in altitude relative to the temperature. Unlike the other two variables, the meridional wind shows some power in the inertial range in the upper troposphere, as well as the strong variability in the low-to-mid troposphere due to easterly waves.

Returning to the inter-relationships between the components, the in-phase relationship between temperature and meridional wind in Figure 7 is supported by the results of cross-spectral analysis (not shown) which show peaks near 16 km in the T-v co-spectrum at periods of 5 and ~10 days. Likewise the quadrature relationship between temperature and zonal wind is reflected by peaks in the T-u quadrature spectrum at 5 days and 17 km and upward to ~20 km and also between 8 and 16 days above 15 km, again peaking at the 16 km level. This pattern of coherence between these components is characteristic of mixed Rossby-gravity waves [*Dunkerton and Baldwin,* 1995] which propagate westward and will rapidly decay with height in the presence of easterly shear. Such is the case with the spectral power in T, u and v in both 2005 and 2007, each of these being in an easterly phase of the Quasi-Biennial Oscillation [*Baldwin et al.,* 2001].

The energy source for the waves is very likely regional deep convection. First, there is the sharp transition at 15 km from vertical coherence in the wind anomalies in the troposphere to downward phase propagation in all components above. This is consistent with energy propagating upward and away from the detrainment level for regional convective systems. Secondly, the coherent wave structure in the UT/LS, while a feature of the summer convective periods in Costa Rica in 2005 and 2007 reported here, was not repeated in the winter of 2006 when we conducted an extended radiosonde campaign at Alajuela in support of the NASA CR-AVE mission. During the winter dry season, deep convection is centered well south of the equator in tropical American longitudes, whereas during summer convection is maximized near the latitude of Costa Rica.

6. Summary and conclusions

The profiles of both water vapor and ozone constituents are consistent with the vertical structure of each of these trace species in the tropics obtained previously with *in situ* water vapor observations by *Vömel et al.* [2002] and ozonesonde observations from SHADOZ [*Thompson et al.* 2003], *viz.,* the TCSP and TC4 mean profiles show an inflection in ozone at 350 K potential temperature and a mean CPT close to 16.6 km and 375 K potential temperature with water vapor volume mixing ratios slightly less than 6 ppmv. Stratospheric minima in the mean profiles of water vapor from TCSP and TC4 were within 0.1 ppmv of 3.1 ppmv. These lay above 19.5 km and 450 K potential temperature, with the latter campaign's minimum 0.8 km and 25 K higher.

Similar to the observations reported in *Vömel et al.* [2002] as well, ice supersaturation was observed on nearly all of the TCSP ascents between 10 km and the CPT, typically in layers several kilometers deep, with embedded regions of supersaturation > 40% observed on several ascents; supersaturated layers were observed in the upper troposphere during TC4 as well, though not as frequently. In both campaigns the saturated layers included a subgroup with significant stratospheric fractions of ozone, and the latter were observed below the 355 K level in both campaigns.

The close spacing of water vapor and ozone profiles we obtained in TCSP, and again in TC4, together with the two months-plus records of high-frequency radiosondes enable us to unequivocally link the structure and variability in the trace constituents to equatorial waves. The profiles in the TCSP and TC4 campaigns each display similar vertical structures in temperature variability, with a marked increase in the variability of temperature at 355 K (14.9 and 14.5 km respectively). This increased variability reflects adiabatic temperature changes associated with a spectrum of equatorial wave motions, including most significantly westward-moving waves with time periods of 4 days and longer. Though not shown explicitly here, ozone anomalies above 15 km were likely also to have been induced by the vertical motion in the waves.

Variability in temperature and ozone mixing ratio and the correlation of peaks in temperature and water vapor mixing ratio suggest that the tropical tropopause layer in the region is distinguished by two characteristics: significant in-mixing of stratospheric air and strong episodes of cooling resulting in dehydration. Temperature and wind anomalies from 4-times daily radiosondes launched during both campaigns demonstrate that these cold episodes are caused by coherent westward-moving wave variations with phase propagation downward from the lower stratosphere to the ~15 km level. These waves produce temperature fluctuations on the order of ±6 K in the stratosphere and are the driver of water vapor variations and dehydration near the tropopause as well as variations of ozone due to vertical displacements across the strong mean gradient. In contrast to this wave-driven regime, below the 15 km level – which is approximately the neutral buoyancy level for deep convection – the waves rapidly weaken with height, and water vapor variations become decoupled from temperature. In this region, the observed supersaturations that are observed are most likely closely associated with detrainment of deep convective clouds and anvils. Similarly, the weakening of wave displacements in this convective regime below 15 km yields a strong decrease in the relative variability of ozone, and vertical mixing is the dominant process.

Water vapor and ozone measurements were made in TCSP during two high-amplitude wave events that dehydrated the air to under 3 ppmv at the CPT. The second event, profiled in the sounding from July 19, is an example of tropopause-level dehydration appearing as the end stage of a process of slow ascent and cooling following deep convective detrainment several days upstream. In TC4 an unusual high amplitude wave event in the first week of August not only pushed cold point water vapor down to 3 ppmv and below, but the accompanying strong subsidence below the cold point produced a 3-km layer of ozone of constant 100 ppbv mixing ratio down to 14 km.

While the data presented here are for two relatively short campaigns, the consistency of the gross characteristics of the temperature, water vapor and ozone between the two argues for the robustness of our results. One important difference between the campaigns is the lower mean RHi in TC4, but this is consistent with the weaker convection overall in TC4 compared to TCSP (see Figures 5-7 in *Pfister et al.* [*op. cit*]). It may also be consistent with the higher mean levels of ozone in the troposphere and its variability in TC4 .

The individual profiles show that there was dehydration of stratospheric air as low as 349 K and as high as 388 K (Figure 4), although these should be considered the lower- and uppermost levels where 'writing' to the atmospheric tape recorder occurred, and we have argued that in this region and season the effective mixing ratio is being set very close to the mean cold point tropopause at 375 K. However, we would also argue that the location of the water vapor tape head close to the mean CPT is not necessarily an indication that dehydration is occurring in layers detrained close to that level. On the contrary, the cooling and lifting produced by the equatorial waves above 15 km is superposed upon an upper troposphere which is in the mean ascending and dehydrating, and the greatest potential for dehydration will thus occur where large temperature excursions in the waves combine with the minimum value of the background temperature profile.

Appendix. The Ticosonde radiosonde collaborations

The Ticosonde/Aura-TCSP and Ticosonde/TC4 radiosonde launch campaigns were the second and fourth in a series of collaborations between investigators from NASA and Costa Rica to make intensive observations of atmospheric variability during the summer rainy season over Central America; the first campaign, Ticosonde/NAME took place in the summer of 2004; a shorter (one-month) sonde campaign was conducted in July 2006 namedTicosonde/Veranillo. All four of these campaigns were focused on characterizing (a) the variability of temperature and winds in the UT/LS from inertial time scales up to the synoptic and (b) regional weather phenomena such as the *veranillo* or midsummer drought [*Magaña, et al.,* 1999] and the Caribbean low-level jet [*Amador,* 1998; *Amador et al.,* 2006; *Amador*, 2008; *Muñoz, et al.*, 2008], as well as temporal fluctuations in the tropical tropopause layer or TTL. Soundings from each campaign directly supported forecasting, flight planning and analysis for the NASA TCSP and TC4 flight campaigns and with the CFH/ECC have also contributed to validation of measurements on board the NASA EOS Aura satellite and other platforms [*e.g., Vömel et al.*, 2007b]. In addition to these four summer season campaigns, there was a winter campaign that took place in early 2006 in conjunction with NAA Costa Rica Aura Validation Experiment (CR-AVE).

Acknowledgments

Funding for the Ticosonde project since 2005 at NASA has been provided through the Radiation Sciences Program, the Upper Atmosphere Research Project, the Atmospheric Chemistry Modeling and Analysis Program and the Climate Dynamics Program. The authors are grateful to Drs. Mark Schoeberl and Anne Douglass of the NASA Aura Science Team without whose support the CFH/SHADOZ Costa Rica launch program would never have become a reality. Dr. Donald Anderson (now at Johns Hopkins University), Dr. Michael Kurylo (now at the University of Maryland, Baltimore County), Dr. Hal Maring of the Radiation Sciences Program were early advocates for and continuing supporters of this collaboration between Costa Rica and the United States. We would like to acknowledge the Costa Rica-USA Foundation (CRUSA) in Costa Rica, the National Science Foundation and the NOAA Office for Global Programs for their support of the Ticosonde/NAME program and Dr. Ramesh Kakar of the NASA Atmospheric Dynamics program for his support for Ticosonde/TCSP. The Ticosonde datasets are a tribute to the enthusiasm and dedication of the launch teams from UNA, UCR and IMN. In this regard, we are especially grateful to Victor Hernández at IMN; Victor Beita, Karla Cerna, Diana Gonzáles, and Jose Pablo Sibaja at UNA; and Kristel Heinrich, Marcial Garbanzo, Gustavo Garbanzo at UCR. We also wish to acknowledge the important contributions in the field by Ticosonde Co-Investigators Drs. Jimena Lopez and Robert Bergstrom of the Bay Area Environmental Research (BAER) Institute, Sonoma, CA, Prof. Patrick Hamill of the San José State University, San José, CA, and Lic. Eladio Zárate, formerly of the National Meteorological Institute of Costa Rica. We are also thankful for the programming support at NASA Ames Research Center by Ms.

Marion Legg and administrative support by Ms. Marion Williams and Mr. Mark Sittloh, all of the BAER Institute. We wish to thank Dr. Pedro León (now at Earth University) and Sr. Gustavo Otárola and their staff at the Costa Rican National Center for High Technology (CeNAT) who provided critical administrative and logistical support, as was also provided by the Regional Environmental Hub at the United States Embassy in San José and Lic. Eladio Zárate and Dr. Max Campos of the Regional Committee on Hydrological Resources (CRRH). Finally, we wish to thank Dr. Joan Alexander of Colorado Research Associates for useful suggestions and assistance in the cross-spectral analysis.

References

Amador, J. (1998), A climatic feature of the tropical Americas: The trade wind easterly jet. *Top. Meteor. y Ocean*. *5*(2), 91-102.

Amador, J. A., E. J. Alfaro, O. G. Lizano, and V. O. Magaña (2006), Atmospheric forcing of the eastern tropical Pacific: A review. *Progress in Oceanography, 69,* 101-142.

Amador, J. A. (2008), The Intra-Americas Seas Low-Level Jet (IALLJ): Overview and Future Research. *Annals of the New York Academy of Sciences*. Trends and Directions in Climate Research, L. Gimeno, R. Garcia, and R. Trigo, Editors,1146(1), 153-188(36).

Baldwin, M. P., et al., (2001), The quasi-biennial oscillation, *Rev. Geophys., 39*(2), 179-229.

Corti, T., B. P. Luo, Q. Fu, H. Vömel, and T. Peter (2006), The impact of cirrus clouds on tropical troposphere-to-stratosphere transport, *Atmos. Chem. Phys.*, *6*, 2539–2547.

Danielsen, E. F. (1982), A dehydration mechanism for the stratosphere, *Geophys. Res. Lett., 9,* 605– 608.

Dunkerton, T. J., and M. P. Baldwin (1995), Observation of 3-6 day meridional wind oscillations over the tropical Pacific, 1973-1992: Horizontal structure, and propagation, *J. Atmos. Sci., 52,* 1585-1601.

Folkins, I., M. Loewenstein, J. Podolske, S. J. Oltmans, and M. Proffitt (1999), A barrier to vertical mixing at 14 km in the tropics: Evidence from ozonesondes and aircraft measurements, *J. Geophys. Res., 104 (D18),* 22,095–22,102.

Folkins, I., C. Braun, A. M. Thompson, and J. Witte (2002), Tropical ozone as an indicator of deep convection, *J. Geophys. Res., 107* (D13), 4184, doi:10.1029/2001JD001178.

Fueglistaler, S., A. E. Dessler, T. J. Dunkerton, I. Folkins, Q. Fu, and P. W. Mote (2009), Tropical tropopause layer, *Rev. Geophys. 47,* RG1004, doi: 10.129/2008RG000267.

Fujiwara, M., F. Hasebe, M. Shiotani, N. Nishi, H. Vömel, and S. Oltmans (2001), Water vapor control at the tropopause by the equatorial Kelvin wave observed over Galapagos, *Geophys. Res. Letts., 28,* 3143-3146.

Gettelman, A., M. L. Salby, and F. Sassi (2002), Distribution and influence of convection in the tropical tropopause region, *J. Geophys. Res., 107* (D10), 4080, doi:10.1029/2001JD001048.

Goff, J. A., and S. Gratch (1946), Low-pressure properties of water from 160 to 212 F, *Trans. Amer. Soc. Heat. Ventilat. Eng., 52,* 95–122.

Halverson, J., *et al,* NASA's Tropical Cloud Systems and Processes Experiment: Investigating tropical cyclogenesis and hurricane intensity change (2007), *Bull. Amer. Meteor. Soc., 88,* 867-882.

Hartmann, D. L., J. R. Holton, and Q. Fu (2001), The heat balance of the tropical tropopause, cirrus, and stratospheric dehydration, *Geophys. Res. Lett.*, *28*, 1969–1972.

Highwood, E. J. and B. J. Hoskins (1998), The tropical tropopause, *Quart. J. Roy. Meteor. Soc.*, *124*, 1579-1604.

Holton, J., and A. Gettelman (2001), Horizontal transport and dehydration of the stratosphere, *Geophys. Res. Lett.*, *28*, 2799–2802.

Jensen, E. J., O. B. Toon, H. B. Selkirk, J. D. Spinhirne, and M. R. Schoeberl (1996), On the formation and persistence of subvisible cirrus clouds near the tropical tropopause, *J. Geophys. Res.*, *101*, 21,361–21,375.

Kley, D., A. L. Schmeltekopf, R. H. Winkler, T. L. Thompson and M. McFarland (1982), Transport of water through the tropical tropopause, *Geophys. Res. Letts., 9*, 617-620.

Komhyr, W. D., R. A. Barnes, G. B. Brothers, J. A. Lathrop, and D. P. Opperman (1995), Electro-chemical concentration cell ozonesonde performance evaluation during STOIC 1989, *J. Geophys. Res., 100,* 9231–9244.

Liu, C., and E. J. Zipser (2005), Global distribution of convection penetrating the tropical tropopause, *J. Geophys. Res.*, *110*, doi:10.1029/2005JD006,063.

Livesey, N. J., *et al.,* Validation of Aura Microwave Limb Sounder O_3 and CO observations in the upper troposphere and lower stratosphere (2008), *J. Geophys. Res., 113,* D15S02, doi:10.1029/2007JD008805.

Magaña, V., J. A. Amador, and S. Medina, The midsummer drought over Mexico and Central America (1999), *J. Clim.*, *12,* 1577-1588.

Mote, P. W., K. H. Rosenlof, M. E. McIntyre, E. S. Carr, J. C. Gille, J. R. Holton, J. S.

Kinnersley, H. C. Pumphrey, J. M. Russell III, and J. W. Waters (1996), An atmospheric tape recorder: The imprint of tropical tropopause temperatures on stratospheric water vapor, *J. Geophys. Res., 101,* 3989–4006.

Mote, P. W., T. J. Dunkerton, M. E. McIntyre, E. A. Ray, P. H.Haynes, and J. M. Russell, III (1998), Vertical velocity, vertical diffusion, and dilution by midlatitude air in the tropical lower stratosphere, *J. Geophys. Res., 103,* 8651-8666, doi:10.1029/98JD00203.

Muñoz, E., A. Busalacchi, S. Nigam and A. Ruiz-Barradas (2008), Winter and summer structure of the Caribbean low-level jet, *J. Clim., 21,* 1260-1276.

Newell, R. E., and S. Gould-Stewart, (1981), A stratospheric fountain?, *J. Atmos. Sci., 38,* 2789-2796.

Pfister, L., H. B. Selkirk, E. J. Jensen, M. R. Schoeberl, O. B. Toon, E. V. Browell, W. B. Grant, B. Gary, M. J. Mahoney, T. V. Bui, E. Hintsa (2001), Aircraft observations of thin cirrus clouds near the tropical tropopause, *J. Geophys. Res., 106*, 9765– 9786.

Pfister, L., H. B. Selkirk, D. O'C. Starr, P. A. Newman, and K. H. Rosenlof, A meteorological overview of the TC4 mission (2010), *J. Geophys. Res*., this special issue.

Plumb, R. A. , and M. Ko (1992), Interrelationships between mixing ratios of long-lived stratospheric constituents, *J. Geophys. Res., 97(9),* 10,145-10,156.

Read, W. G., D. L. Wu, J. W. Waters, and H. C. Pumphrey (2004), Dehydration in the tropical tropopause layer: Implications from the UARS Microwave Limb Sounder, *J. Geophys. Res., 109*, D06110,doi:10.1029/2003JD004056.

Read, W. G., *et al.,* Aura Microwave Limb Sounder upper tropospheric and lower stratospheric H2O and relative humidity with respect to ice validation (2007), *J. Geophys. Res., 112*, D24S35, doi:10.1029/2007JD008752.

Reed, R. J., and C. L. Vleck, (1969) The annual variation in the tropical lower stratosphere, *J. Atmos. Sci., 26*, 163-179.

Reid, G. C., and K. S. Gage (1981), On the annual variation in the height of the tropical tropopause, *J. Atmos. Sci., 38*, 1928-1938.

Reid, G. C., and K. S. Gage (1996), The tropical tropopause over the western Pacific: Wave driving, convection, and the annual cycle, *J. Geophys. Res., 101(16),* 21,233-

21,241.

Rosenlof, K. H., and G. C. Reid, Trends in the temperature and water vapor content of the tropical lower stratosphere: Sea surface connection (2008), *J. Geophys. Res.*, *113*, D06107, doi:10.1029/2007JD009109.

Schoeberl, M. R., B. N. Duncan, A. R. Douglass, J. Waters, W. Read and M. Filipiak (2006), The carbon monoxide tape recorder, *Geophys. Res. Letts., 33,* L12811, doi:10.1029/2006GL026178.

Schoeberl, M. R., A. R. Douglass, R. S. Stolarski, S. Pawson, S. E. Strahan, and W. Read (2008), Comparison of lower stratospheric tropical mean vertical velocities, *J. Geophys. Res.*, *113*, doi:10.1029/2008JD010221.

Seidel, D. J., R. J. Ross, J. K. Angell, and G. C. Reid (2001), Climatological characteristics of the tropical tropopause as revealed by radiosondes, *J. Geophys. Res., 106,* 7587-7878.

Selkirk, H. B. (1993), The Tropopause cold trap in the Australian monsoon during STEP/AMEX 1987, *J. Geophys. Res., 98(D5),* 8591–8610.

Sherwood, S. C., and A. E. Dessler (2001), A model for transport across the tropical tropopause, *J. Atmos. Sci., 58*, 765– 779, 2001.

Sparling, L., and M. Schoeberl (1995), Mixing entropy analysis of dispersal of aircraft emissions in the lower stratosphere, *J. Geophys. Res.,* **100**, 16805-16812.

Thompson, A. M., Southern Hemisphere Additional Ozonesondes (SHADOZ) 1998–2000 tropical ozone climatology. 1. Comparison with Total Ozone Mapping Spectrometer (TOMS) and ground-based measurements (2003), *J. Geophys. Res., 108* (D2), 8238, doi:10.1029/2001D000967.

Toon, B., *et al.,* Planning and implementation of the Tropical Composition, Cloud and Climate Coupling Experiment (TC4). *J. Geophys. Res.,* this special issue.

Vömel, H., S. J. Oltmans, B. J. Johnson, F. Hasebe, M. Shitoani, M. Fujiwara, N. Nishi, M. Agama, J. Cornejo, F. Paredes and H. Enriquez (2002), Balloon-borne observations of water vapor and ozone in the tropical upper troposphere and lower stratosphere, *J. Geophys. Res., 107* (D14), 4210, doi:10.1029/2001JD000707.

Vömel, H., D. E. David, and K. Smith, Accuracy of tropospheric and stratospheric water vapor measurements by the cryogenic frost point hygrometer: Instrumental details and observations (2007a), *J. Geophys. Res., 112,* D08305, doi:10.1029/2006JD007224.

Vömel, H., et al. (2007b), Validation of Aura Microwave Limb Sounder water vapor by balloon-borne Cryogenic Frost point Hygrometer measurements, *J. Geophys. Res., 112,* D24S37, doi:10.1029/2007JD008698.

Vömel, H., H. Selkirk, L. Miloshevich, J. Valverde, J. Valdés, E. Kyrö, R.Kivi, W. Stolz, G. Peng, and J. A. Diaz (2007c), Radiation dry bias of the Vaisala RS92 humidity sensor, *J. Atmos. Oceanic Technol., 24*, 953–963.

Wang, P.-H., P. Minnis, M. P. McCormick, G. S. Kent, and K. M. Skeens (1996), A 6-year climatology of cloud occurrence frequency from Stratospheric Aerosol and Gas Experiment II observations (1985–1990), *J. Geophys. Res., 101(D23),* 29,407–29,429.

Waters, J.W., *et al.,* The Earth Observing System Microwave Limb Sounder (EOS MLS) on the Aura satellite (2006), *IEEE Trans. Geosci. Remote Sensing*, *44*, 1075-1092.

Wheeler, M., G. N. Kiladis, P. J. Webster (2000), Large-scale dynamical fields associated with convectively coupled equatorial waves, *J. Atmos. Sci., 57(5),* 613-640.

Yulaeva, E., J. R. Holton, and J. M. Wallace (1994), On the cause of the annual cycle in tropical lower-stratospheric temperature *J. Atmos. Sci., 51,* 169-174.

Figure captions

Figure 1: TCSP (left) and TC4 (right) mean profiles of temperature (heavy solid) and ozone mixing ratio (heavy dotted) calculated on a grid with 50-m resolution, each bracketed by campaign minima and maxima at each grid level. Light dotted lines at right are profiles of the full range of temperatures in each campaign. Inverted triangles mark the mean altitude and temperature of the CPT.

Figure 2: Variance of (a) temperature and (b) ozone mixing ratio and (c) standard and fractional deviations (see text) of CFH water vapor mixing ratio plotted against potential temperature. Horizontal lines are mean altitudes of the CPT from each campaign.

Figure 3: At left in each panel: CFH water vapor volume mixing ratio data color-coded by relative humidity with respect to ice (RHi), mean profile (heavy dark line) and envelope of ± 1 standard deviation (light lines), and mean saturation mixing ratio (dotted red line). The mean cold point is shown by the inverted triangle, color coded by RHi. At right, mean profile of RHi (blue/white) and envelope of RHi maxima and minima. All profiles with the exception of RHi maxima and minima are smoothed with an 11-pt boxcar filter.

Figure 4: RHi observations from (a) TCSP and (b) TC4, color-coded by ozone mixing ratio. The middle of the color scale (white) is set to the highest tropospheric ($\theta \leq 345$ K) ozone observed in each campaign and full red set to the average tropospheric ozone mixing ratio. Inverted triangles centered at the mean cold point tropopause, horizontal (vertical) bars extend to maximum and minimum values of RHi (pressure) during each campaign.

Figure 5: Selected ascents from the 2005 TCSP CFH/ECC campaign. Water vapor mixing ratio, heavy dots color-coded by relative humidity with respect to ice; mean water vapor mixing ratio, dotted black line; ozone mixing ratio, red line; mean ozone mixing ratio, smooth red line; and saturation mixing ratio of water, continuous black line. Soundings on (a) July 11, (b) July 13, (c) July 16, (d) July 19, (e) July 23 and (f) July 25.

Figure 6: Mean profiles of zonal (blue) and meridional (red) winds in envelopes of ± 1 standard deviation. Data from four-times-daily radiosondes at Alajuela over the two-month period 16 June through 15 August, 2005.

Figure 7: Time-height cross-section of anomalies at Alajuela, 16 June -15 August 2005, of (a) temperature, (b) zonal wind and (c) meridional wind. Heavy dashed lines in all three panels are phase lines of negative temperature anomalies, dotted, positive anomalies. Horizontal dotted lines at TCSP campaign (July 8-25) mean altitudes of the 350 and 355 K surface, and heavier dotted line at the mean altitude of the CPT.

Figure 8: Time series of saturation mixing ratio at the cold point from radiosonde measurements at Alajuela, 16 June through 15 August 2005 – light dotted line, spline-interpolated data, heavy line, binomially-smoothed (N=51). Large dots are cold point water vapor volume mixing ratio from the CFH.

Figure 9: Frequency-height cross-sections of power spectral density from periodogram analysis for anomalies at Alajuela, 16 June -15 August 2005, of (a) temperature, (b) zonal wind and (c) meridional wind. Equivalent periods in days are shown across the top; f_i marks the inertial period at 10°N.

Flight	***Day***	***Time (UT)***	***Max altitude (km)***			***Flight***	***Day***	***Time (UT)***	***Max altitude (km)***	
			Ozone	***WV***					***Ozone***	***WV***
Ticosonde/Aura-TCSP 2005						SJ022	7/24	17:23	21.0	21.0
SJ001	7/8	18:08	30.2	11.0		**SJ023**	**7/25**	**5:34**	**30.8**	**–**
SJ002	7/9	17:54	30.3	12.6		SJ024	7/25	17:27	28.7	21.8
SJ003	7/10	17:58	31.7	8.5		***Ticosonde/TC^4 2007***				
SJ004	7/11	18:14	31.1	21.0		SJ132	7/2	17:48	27.3	26.4
SJ005	7/12	18:10	30.5	21.6		SJ135	7/16	18:25	30.3	21.4
SJ006	7/13	18:06	31.6	24.4		SJ136	7/19	17:57	32.1	21.0
SJ007	7/14	18:15	31.4	12.6		SJ137	7/22	17:48	30.4	21.3
SJ008	7/15	17:54	32.2	17.8		SJ138	7/25	17:05	32.0	20.1
SJ009	7/16	18:12	30.7	24.1		SJ139	7/28	17:36	14.0	14.0
SJ010	7/17	17:40	30.3	20.7		SJ140	7/31	17:20	31.7	31.7
SJ011	7/18	17:43	30.1	12.6		**SJ141**	**8/2**	**05:39**	**30.1**	**17.0**
SJ012	7/19	17:34	30.1	25.0		SJ142	8/3	15:42	31.2	27.7
SJ013	7/20	18:46	27.3	18.5		**SJ143**	**8/4**	**05:20**	**28.8**	**18.1**
SJ014	**7/21**	**5:58**	**19.1**	**12.3**		**SJ144**	**8/5**	**05:32**	**30.0**	**17.1**
SJ015	7/21	17:39	29.4	4.9		**SJ145**	**8/7**	**05:31**	**28.9**	**17.3**
SJ016	**7/22**	**5:28**	**30.5**	**23.5**		SJ146	8/8	17:36	30.7	23.9
SJ017	7/22	17:33	30.2	19.3		**SJ147**	**8/09**	**05:29**	**29.3**	**23.0**
SJ018	**7/23**	**5:28**	**18.6**	**14.8**		SJ148	8/13	14:50	27.4	24.7
SJ020	7/23	18:47	31.8	27.5		SJ149	8/30	17:07	32.3	21.9
SJ021	**7/24**	**5:34**	**30.6**	**25.1**						

Table 1: Flight statistics for CFH/ECC launches during the July 2005 Ticosonde/Aura-TCSP campaign and July-August 2007 Ticosonde/TC4 campaign. Flights in bold are nighttime ascents.

	Instrument	Units	Average	Standard Deviation	Minimum (or lowest)	Maximum (or highest)	n
TCSP 8-25 Jul 2005							
Altitude	RS80	km	16.64	0.65	15.80	18.26	23
Pressure	RS80	hPa	99.9	10.6	114.6	75.2	23
Temperature	RS80	°C	-79.2	2.48	-85.0	-76.2	23
Potential temperature	RS80	K	375.3	13.6	360.1	403.9	23
Ozone mixing ratio	ECC	ppmv	0.158	0.064	0.056	0.288	22
Water vapor mixing ratio	CFH	ppmv	5.73	1.72	2.62	8.23	13
Saturation mixing ratio	RS80	ppmv	6.76	2.61	2.29	11.3	23
RH_{ice}	CFH/RS80	%	88.4	28.4	47.3	134.6	13
TC4 2 Jul – 30 Aug 2007							
Altitude	RS80	km	16.64	0.56	15.78	17.55	15
Pressure	RS80	hPa	99.6	9.74	114.8	85.0	15
Temperature	RS80	°C	-78.9	1.69	-83.0	-77.0	15
Potential temperature	RS80	K	376.0	10.6	360.5	395.3	15
Ozone mixing ratio	CFH	ppmv	0.145	0.0366	0.097	0.23	15
Water vapor mixing ratio	ECC	ppmv	5.79	1.28	3.87	8.08	15
Saturation mixing ratio	RS80	ppmv	6.79	1.77	3.44	9.39	23
RH_{ice}	CFH/RS80	%	89.0	21.9	53.9	119.3	15

Table 2: CPT statistics for the TCSP and TC4 water vapor/ozonesonde flight series.

	Instrument	**Units**	**Average**	**Standard Deviation**	**Minimum (or lowest)**	**Maximum (or highest)**	**N**
TCSP – Jul 2005							
Altitude	RS80	km	19.5	0.72	18.3	20.7	12
Pressure	RS80	hPa	62.1	7.24	74.5	50.0	12
Temperature	RS80	°C	-69.5	2.63	-72.6	-64.5	12
Potential temperature	RS80	K	451.6	19.7	423.3	486.5	12
Water vapor	CFH	ppmv	3.21	0.47	2.7	4.4	12
Ozone	ECC	ppmv	0.79	0.27	0.464	1.36	12
TC4 – Jul/Aug 2007							
Altitude	RS80	km	20.3	1.12	19.0	23.0	11
Pressure	RS80	hPa	54.3	9.45	65.9	34.7	11
Temperature	RS80	°C	-67.2	3.22	-71.9	-61.4	11
Potential temperature	RS80	K	476.7	33.4	443.2	553.2	11
Water vapor	ECC	ppmv	3.02	0.56	1.84	3.57	11
Ozone	CFH	ppmv	1.27	0.772	0.66	3.25	11

Table 3: Profile minimum water vapor statistics for the TCSP and TC4 water vapor and ozonesonde campaigns.

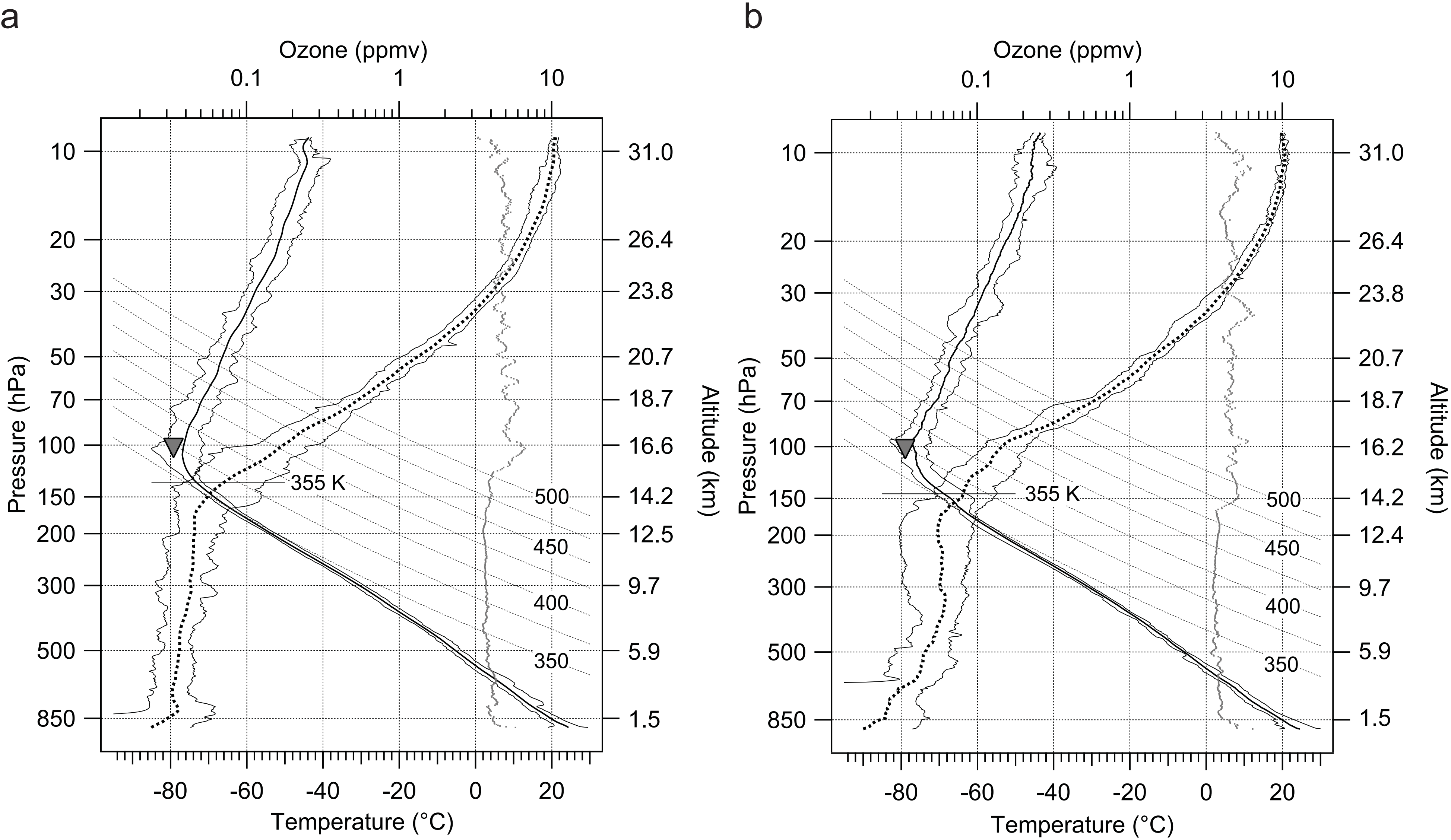

Figure 1: TCSP (left) and TC4 (right) mean profiles of temperature (heavy solid) and ozone mixing ratio (heavy dotted) calculated on a grid with 50-m resolution, each bracketed by the minima and maxima observed at each grid level in the campaign. Light dotted lines at right are profiles of the full range of temperatures in the each campaign. Inverted triangles mark the mean altitude and temperature of the cold point tropopause.

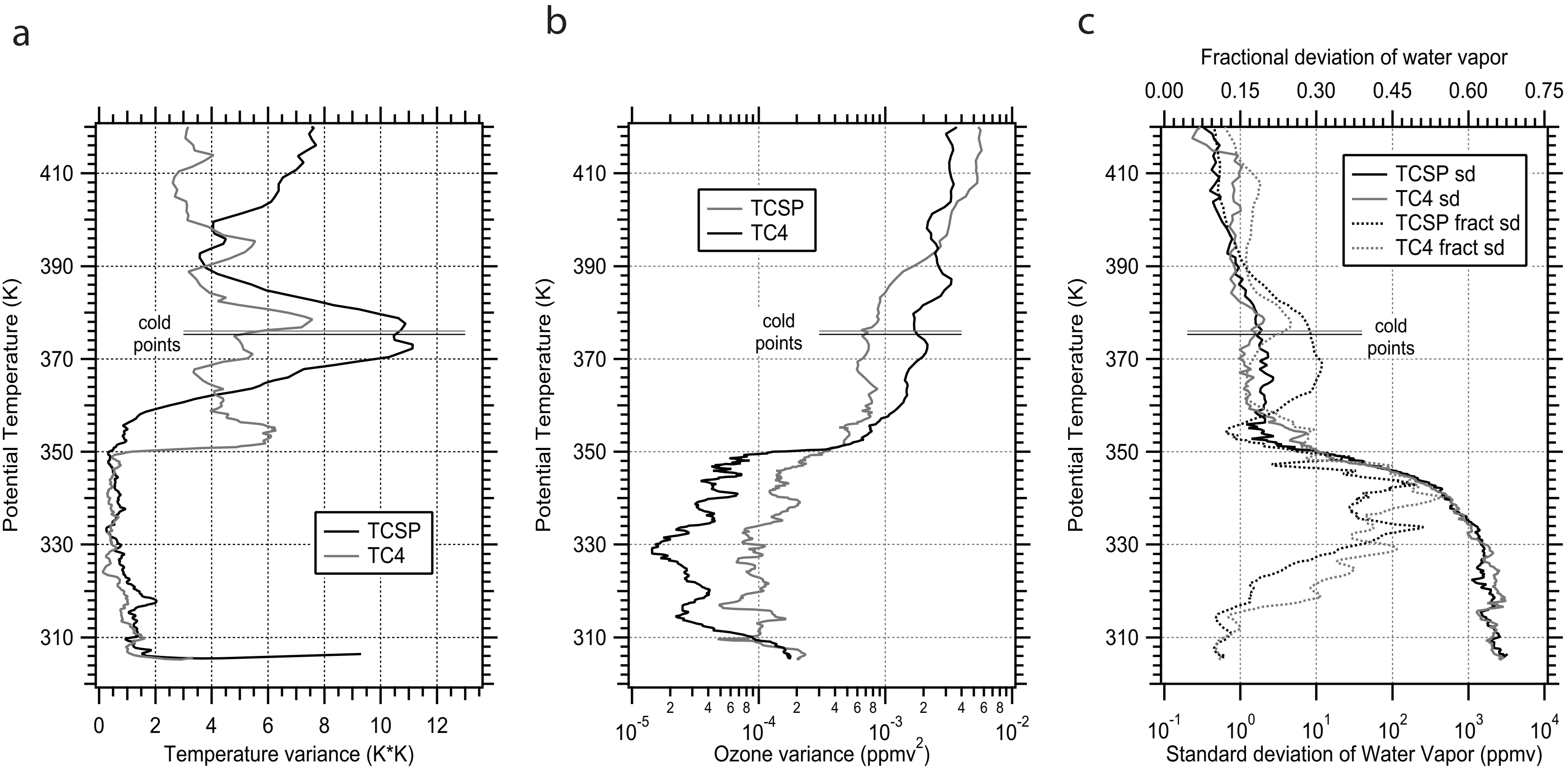

Figure 2: Variance of (a) temperature and (b) ozone mixing ratio and (c) standard and fractional deviations (see text) of CFH water vapor mixing ratio plotted against potential temperature. Horizontal lines are mean altitudes of the cold point tropopause from each campaign.

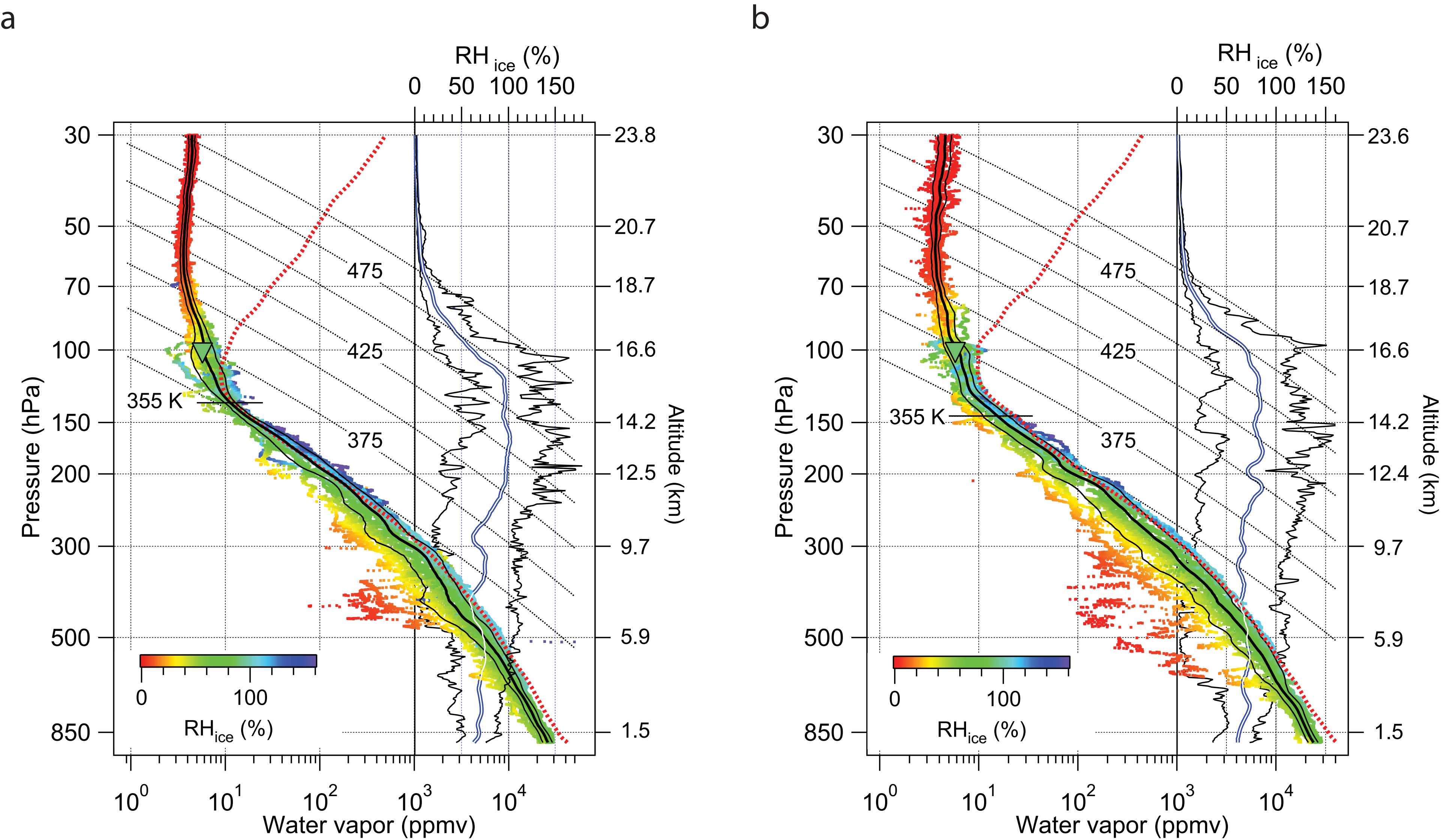

Figure 3: At left in each panel: CFH water vapor volume mixing ratio data color-coded by RHi, and mean profile (heavy dark line) and envelope of ± 1 standard deviation envelope (light lines), mean saturation mixing ratio (dotted red line), mean cold point inverted triangle, color coded by RHi. At right, mean profile of RHi (blue/white) and envelope of RHi maxima and minima. All profiles with the exception of RHi maxima and minima smoothed with an 11-pt boxcar filter.

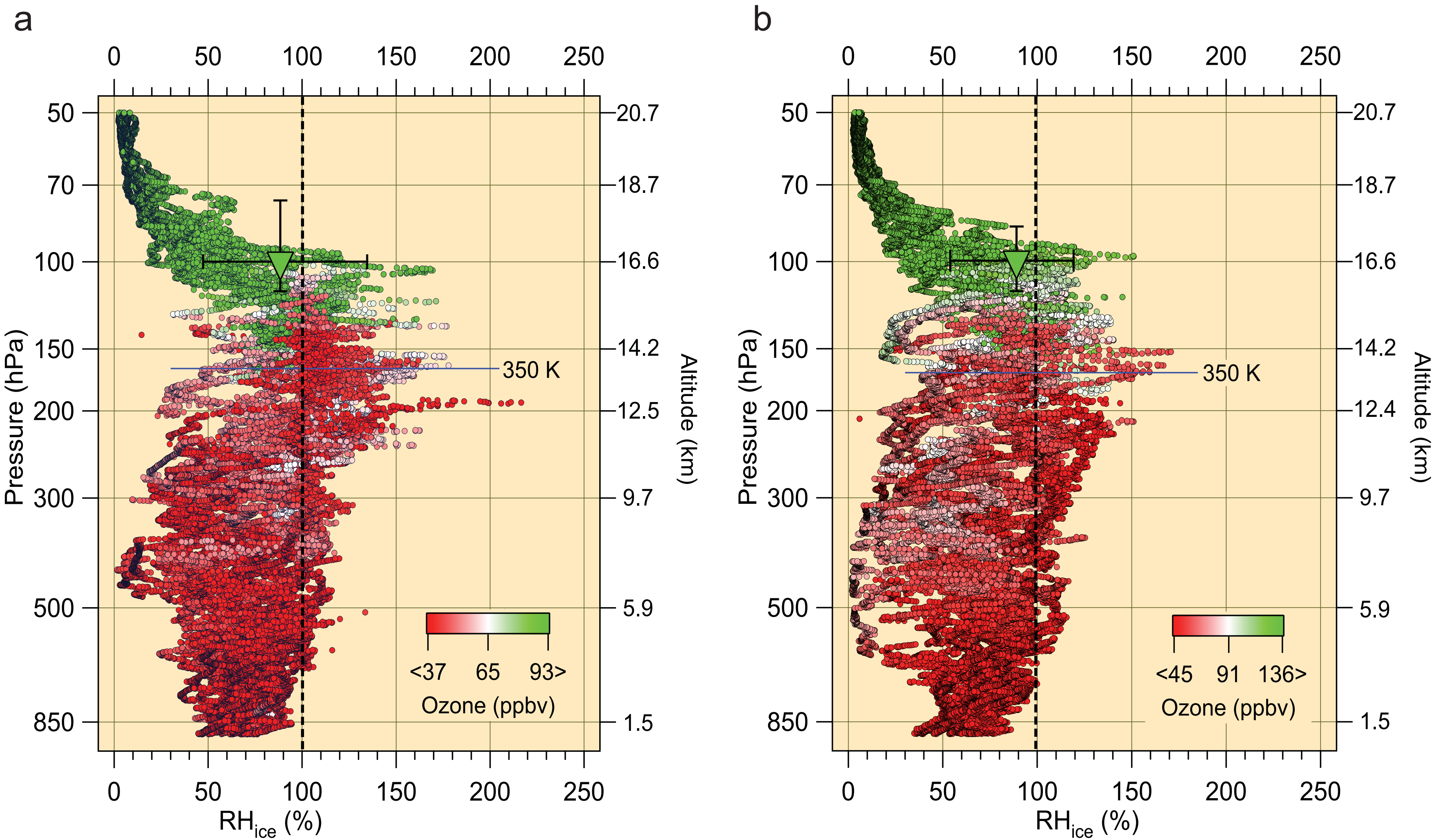

Figure 4: Observations of relative humidity with respect to ice (RHi) from (a) TCSP and (b) TC4, color-coded by ozone mixing ratio. The middle of the color scale (white) is set to the highest tropospheric ($\theta \leq 345$ K) ozone observed in each campaign and full red set to the average tropospheric ozone mixing ratio. Inverted triangles centered at the mean cold point tropopause, horizontal (vertical) bars extend to maximum and minimum values of RHi (pressure) during each campaign.

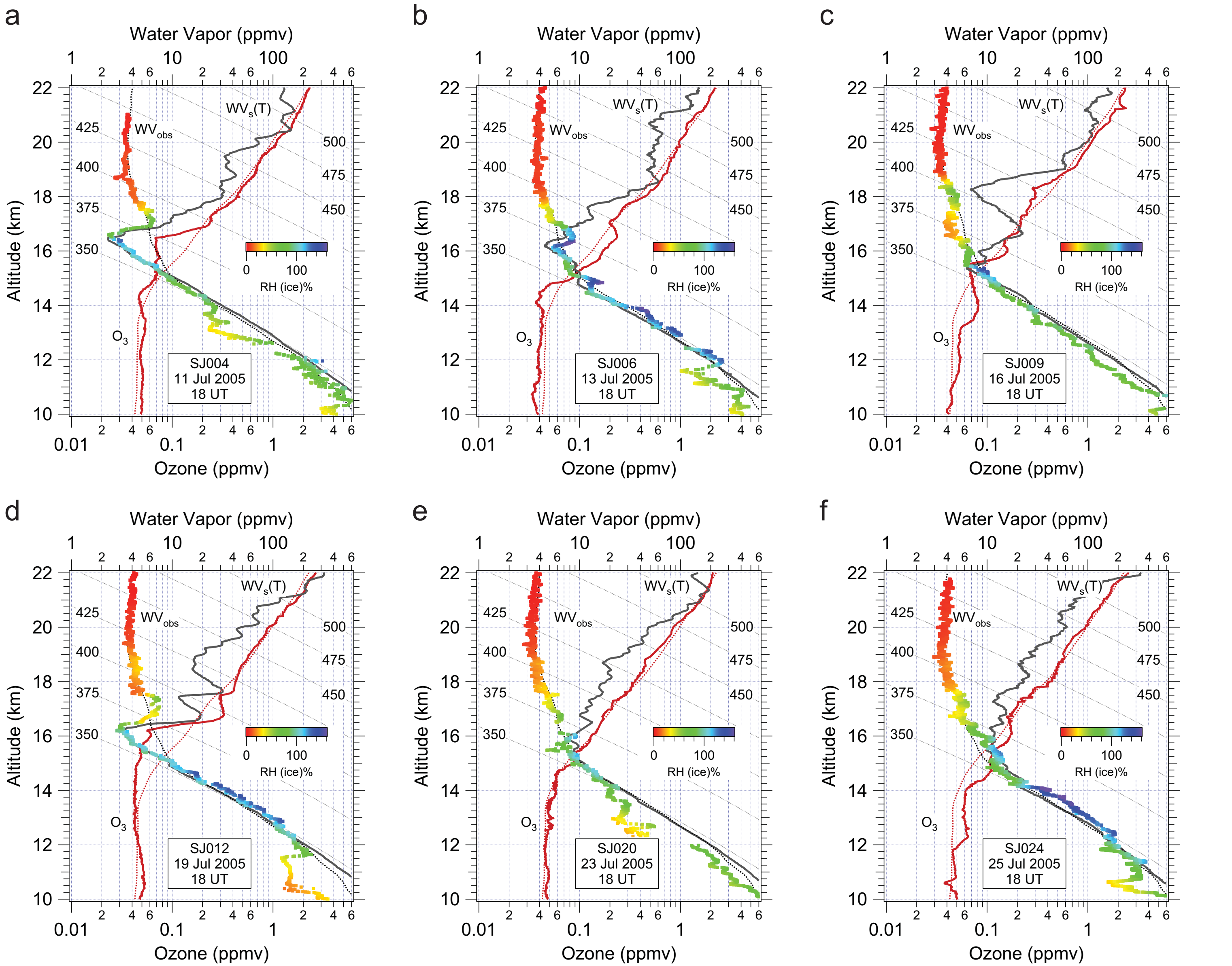

Figure 5: Selected ascents from the 2005 TCSP CFH/ECC campaign. Water vapor mixing ratio, heavy dots color-coded by relative humidity with respect to ice; mean water vapor mixing ratio, dotted black line; ozone mixing ratio, red line; mean ozone mixing ratio, smooth red line; and saturation mixing ratio of water, continuous black line. Soundings on (a) July 11, (b) July 13, (c) July 16, (d) July 19, (e) July 23 and (f) July 25.

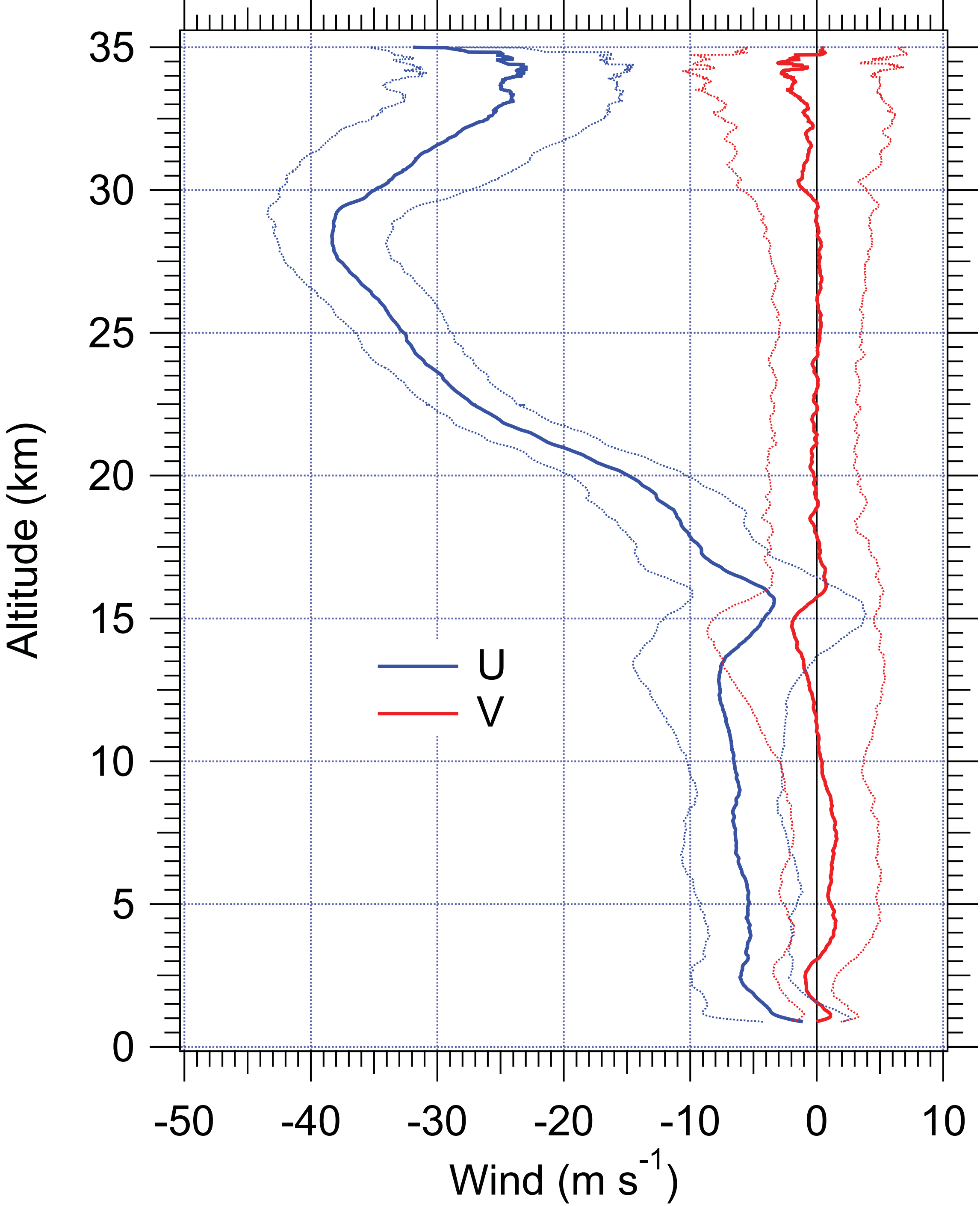

Figure 6: Mean profiles of zonal (blue) and meridional (red) winds in envelopes of ± 1 standard deviation. Data from four-times-daily radiosondes at Alajuela over the two-month period 16 June through 15 August, 2005.

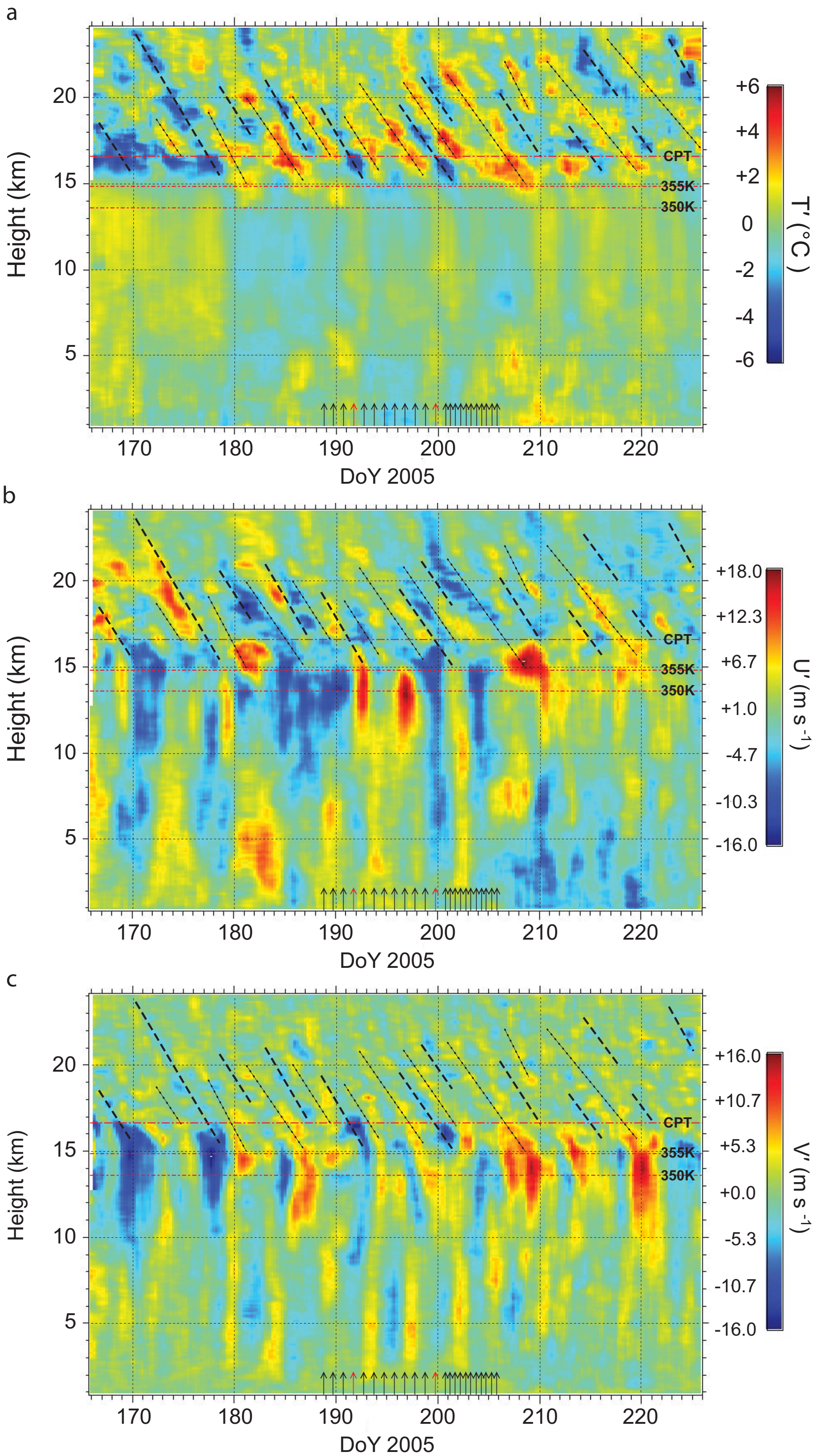

Figure 7: Time-height cross-section of anomalies at Alajuela, 16 June -15 August 2005, of (a) temperature, (b) zonal wind and (c) meridional wind. Heavy dashed lines in all three panels are phase lines of negative temperature anomalies, dotted, positive anomalies. Horizontal dotted lines at TCSP campaign (July 8-25) mean altitudes of the 350 and 355 K surface, and heavier dotted line at the mean altitude of the cold point tropopause.

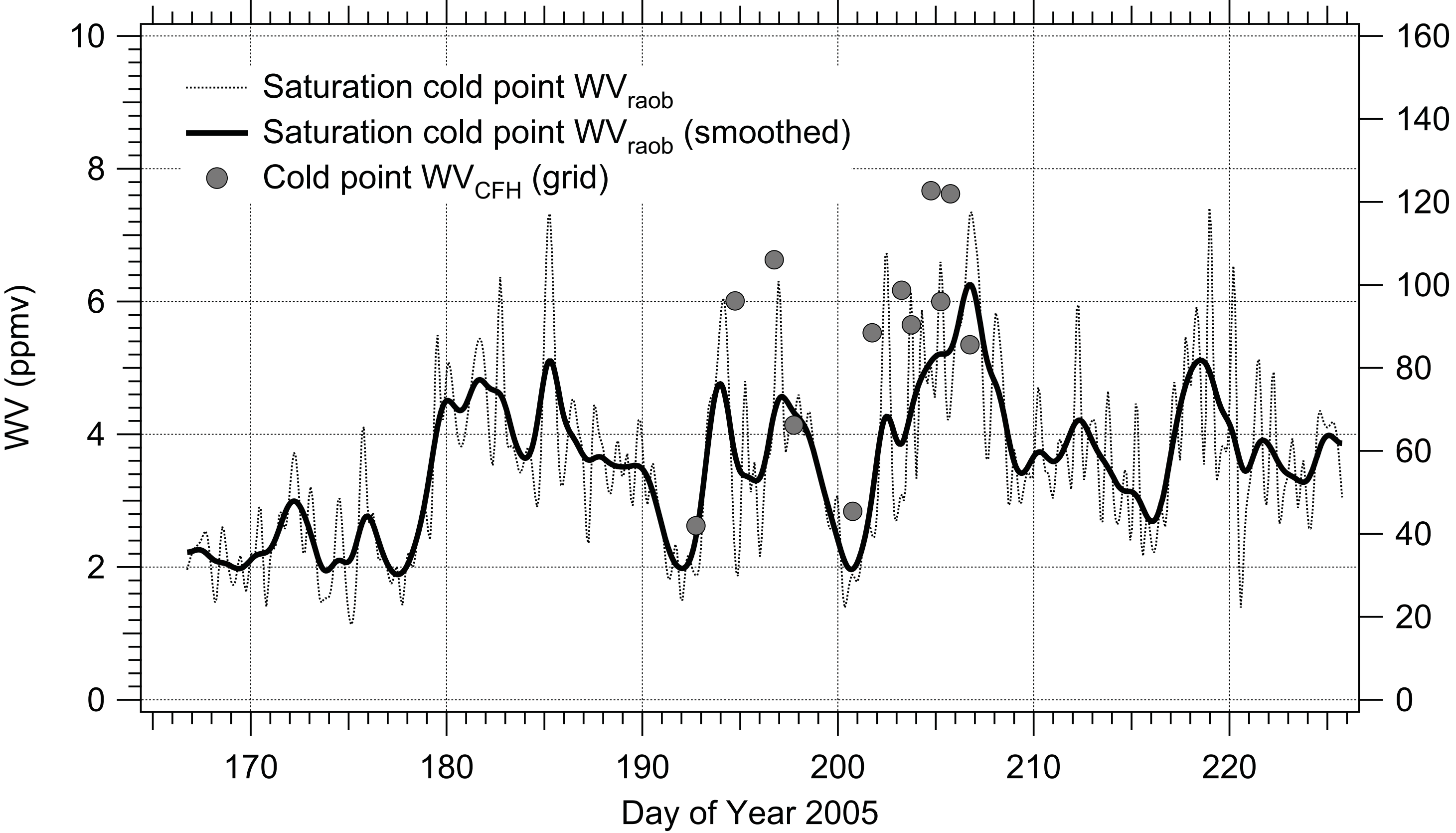

Figure 8: Time series of saturation mixing ratio at the cold point from radiosonde measurements at Alajuela, 16 June through 15 August 2005 – light dotted line, spline-interpolated data, heavy line, binomially-smoothed (N=51). Large dots are cold point water vapor volume mixing ratio from the CFH.

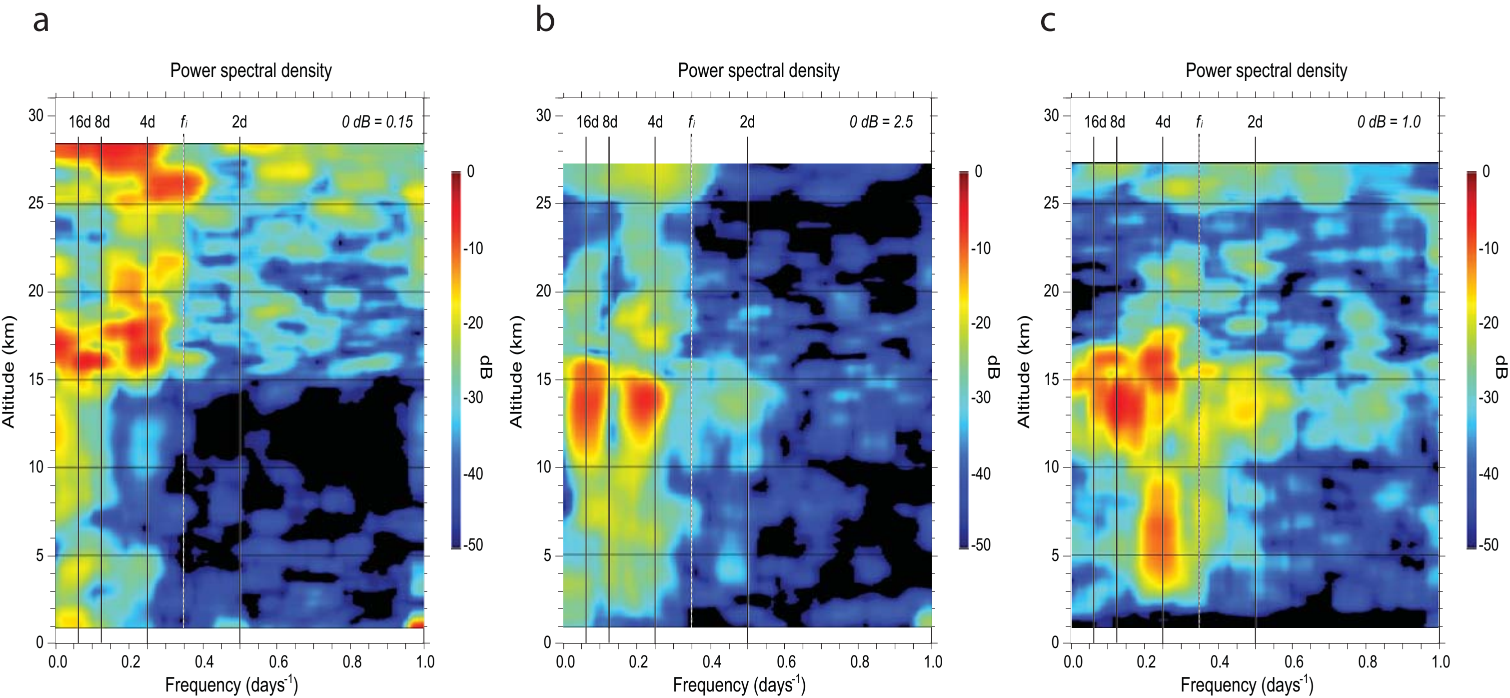

Figure 9: Frequency-height cross-sections of power spectral density from periodogram analysis for anomalies at Alajuela, 16 June -15 August 2005, of (a) temperature, (b) zonal wind and (c) meridional wind. Equivalent periods in days are shown across the top; fi marks the inertial period at 10°N.